12-6-2014

Free-breathing Pulmonary (1)H and Hyperpolarized (3)He MRI: Comparison in COPD and Bronchiectasis.

Dante P I Capaldi
Western University, dcapald@uwo.ca

Khadija Sheikh
Western University, ksheikh6@uwo.ca

Fumin Guo
Western University, fguo24@uwo.ca

Sarah Svenningsen
Western University, ssvenni2@uwo.ca

Roya Etemad-Rezai
Western University, roya.etemadrezai@lhsc.on.ca

See next page for additional authors

Authors
Dante P I Capaldi, Khadija Sheikh, Fumin Guo, Sarah Svenningsen, Roya Etemad-Rezai, Harvey O Coxson, Jonathon A Leipsic, David G McCormack, and Grace Parraga

Original Investigations

Free-breathing Pulmonary ^{1}H and Hyperpolarized ^{3}He MRI:

Comparison in COPD and Bronchiectasis

Dante P. I. Capaldi, BSc, Khadija Sheikh, BSc, Fumin Guo, MEng, Sarah Svenningsen, BMSc, Roya Etemad-Rezai, MD, FRCPC, Harvey O. Coxson, PhD, Jonathon A. Leipsic, MD, David G. McCormack, MD, FRCPC, Grace Parraga, PhD

Rationale and Objectives: In this proof-of-concept demonstration, we aimed to quantitatively and qualitatively compare pulmonary ventilation abnormalities derived from Fourier decomposition of free-breathing ^{1}H magnetic resonance imaging (FDMRI) to hyperpolarized ^{3}He MRI in subjects with chronic obstructive pulmonary disease (COPD) and bronchiectasis.

Materials and Methods: All subjects provided written informed consent to a protocol approved by a local research ethics board and Health, Canada, and they underwent MRI, computed tomography (CT), spirometry, and plethysmography during a single 2-hour visit. Semiautomated segmentation was used to generate ventilation defect measurements derived from FDMRI and ^{3}He MRI, and these were compared using analysis of variance and Pearson correlations.

Results: Twenty-six subjects were evaluated including 12 COPD subjects (67 $\pm$ 9 years) and 14 bronchiectasis subjects (70 $\pm$ 11 years). For COPD subjects, FDMRI and ^{3}He MRI ventilation defect percent (VDP) was 7 $\pm$ 6% and 24 $\pm$ 14%, respectively ($P < .001$; bias = $-16 \pm 9\%$). In COPD subjects, FDMRI was significantly correlated with ^{3}He MRI VDP ($r = .88$; $P = .0001$), ^{3}He MRI apparent diffusion coefficient ($r = .71$; $P < .05$), airways resistance ($r = .60$; $P < .05$), and RA_{950} ($r = .80$; $P < .01$). In subjects with bronchiectasis, FDMRI VDP (5 $\pm$ 3%) and ^{3}He MRI VDP (18 $\pm$ 9%) were significantly different ($P < .001$) and not correlated ($P > .05$). The Dice similarity coefficient (DSC) for FDMRI and ^{3}He MRI ventilation was 86 $\pm$ 7% for COPD and 86 $\pm$ 4% for bronchiectasis subjects ($P > .05$); the DSC for FDMRI ventilation defects and CT RA_{950} was 19 $\pm$ 20% in COPD and 2 $\pm$ 3% in bronchiectasis subjects ($P < .01$).

Conclusions: FDMRI and ^{3}He MRI VDP were strongly related in COPD but not in bronchiectasis subjects. In COPD only, FDMRI ventilation defects were spatially related with ^{3}He ventilation defects and emphysema.

Key Words: Fourier decomposition; magnetic resonance imaging; bronchiectasis; chronic obstructive pulmonary disease.

Acad Radiol 2014; ■:1–10

From the Imaging Research Laboratories, Robarts Research Institute, 1151 Richmond Street North, London, Ontario, Canada N6A 5B7 (D.P.I.C., K.S., F.G., S.S., G.P.); Department of Medical Biophysics, The University of Western Ontario, London, Ontario, Canada (D.P.I.C., K.S., S.S., G.P.); Graduate Program in Biomedical Engineering, The University of Western Ontario, London, Ontario, Canada (F.G., G.P.); Department of Medical Imaging, The University of Western Ontario, London, Ontario, Canada (R.E.R., G.P.); James Hogg Research Centre, University of British Columbia, Vancouver, British Columbia, Canada (H.O.C., J.A.L.); and Division of Respirology, Department of Medicine, The University of Western Ontario, London, Ontario, Canada (D.G.M.). Received September 4, 2014; accepted October 3, 2014. Funding Sources: The authors gratefully acknowledge funding from Canadian Institutes of Health Research (CIHR) Team Grant for the Thoracic Imaging Network of Canada, CIHR operating grant MOP# 106437, and the Canadian Respiratory Research Network (CRRN). G.P. also gratefully acknowledges salary support from CIHR New Investigator award. **Address correspondence to:** G.P. e-mail: gparraga@robarts.ca

http://dx.doi.org/10.1016/j.acra.2014.10.003

Chronic obstructive pulmonary disease (COPD) is diagnosed and disease severity stratified based on irreversible airflow obstruction measured using spirometry. Airflow obstruction, symptoms, and exercise capacity measurements in COPD are related to both parenchyma destruction (emphysema) and airway remodeling (airways disease and bronchiectasis) (1,2). Although spirometry is relatively easy to implement, reproducible, and inexpensive, it can only provide a global measure of lung function and is weakly predictive of COPD progression, as well as insensitive to early disease stages (3–5). The limitations of spirometry measurements of COPD have motivated the development of thoracic imaging approaches to provide direct and regional measurements of the underlying pathologic features of COPD—airways disease and emphysema.

High-resolution computed tomography is the clinical imaging tool of choice for visualizing and quantifying airways disease (6,7) and emphysema (8–10) in patients with COPD. Emphysema can be quantified automatically based on thresholds of the CT density histogram (<−950 Hounsfield units [HU]) (8,10,11). Thoracic CT estimates of airways disease can also be generated using measurements of airway wall area percent (WA%) and lumen area (LA). Indirect measurements of airways disease include CT measurements of gas trapping using densitometry thresholds (−856 HU) on expiratory CT images (12) or parametric response maps using coregistered inspiratory and expiratory CT (13). Finally, bronchiectasis can be readily observed in thoracic CT in up to 50% of patients with severe COPD (14,15), and this is typically identified by enlarged bronchial diameters and evidence of significant mucous plugging.

Pulmonary magnetic resonance imaging (MRI) using inhaled hyperpolarized ^{3}He or ^{129}Xe gas also provides a way to visualize regional ventilation abnormalities and lung microstructure in subjects with COPD (16–25). Ventilation abnormalities may be quantified using the ventilation defect percent (VDP), that represents the volume of ventilation defects normalized to the thoracic cavity (24,26). Although rapid (8–15 seconds acquisition time) and well tolerated, inhaled noble gas MRI is dependent on polarized gas and multinuclear magnetic resonance imaging hardware. An alternative approach that exploits Fourier decomposition of free-breathing pulmonary MRI (FDMRI) was first developed by Bauman et al. (27) at 1.5 T. This method provides a way to generate quantitative pulmonary maps of ventilation and perfusion using fast pulmonary MRI acquisitions of free-breathing ^{1}H MRI and nonrigid registration (27–33). FDMRI was recently compared and validated with single-photon emission computed tomography (SPECT)-CT (28) and ^{3}He MRI (30) in a porcine model.

Until now, FDMRI has not been evaluated in subjects with COPD or bronchiectasis, nor at 3 Twhere there is diminished signal intensity at higher field strengths owing to T2★ effects (34). Hence, our objective was to generate FDMRI (first developed at 1.5 T) and ^{3}He MRI ventilation measurements acquired at 3 T in subjects with COPD or bronchiectasis. We hypothesized that ventilation defects measured using FDMRI and ^{3}He MRI would be spatially and quantitatively correlated in subjects with COPD and those with bronchiectasis.

MATERIALS AND METHODS

Study Subjects

All subjects were previously diagnosed with COPD or bronchiectasis by a pulmonologist and provided written informed consent to the study protocol approved by a local research ethics board and Health Canada. Subjects with COPD were classified according to the Global initiative for chronic Obstructive Lung Disease (GOLD) grades (1). COPD subjects were ex-smokers aged between 50 and 80 years and with a smoking history of ≥10 pack years. Subjects with bronchiectasis were ex-smokers (n = 4) and never-smokers (n = 10) aged between 40 and 85 years. An expert chest radiologist (>20 years experience) qualitatively examined CT data for evidence of bronchiectasis and emphysema.

Pulmonary Function Tests

Spirometry and whole-body plethysmography were performed using a body plethysmograph (MedGraphics Corporation, St. Paul, MN) to measure the forced expiratory volume in 1 second, forced vital capacity, and static lung volumes including total lung capacity, inspiratory capacity, residual volume, and functional residual capacity (FRC), airways resistance (R_{aw}), and the diffusing capacity of lung for carbon monoxide (DL_{CO}) using the attached gas analyzer. All measurements were performed according to the American Thoracic Society guidelines (35).

Image Acquisition

MRI was performed with a whole-body 3 T Discovery MR750 system (General Electric Health Care, [GEHC] Milwaukee, WI) capable of performing broadband imaging. All MR images were acquired in the coronal slice orientation. Conventional ^{1}H MRI was performed 5 minutes before hyperpolarized ^{3}He MRI. Subjects were instructed to maintain normal tidal breathing and then from FRC inhale a 1.0 L mixture of ^{4}He/N_2. For the purposes of this study and to aid direct comparisons, all MRI and CT images were acquired at FRC + 1.0 L for consistency. By having all subjects inhale 1.0 L of gas after passive expiration, we ensured consistent lung volumes across all imaging methods. We also note that to truly capture the same lung volume consistently, our approach of using a measured volume for inhalation is straightforward and easily undertaken even supine in the CT or MR scanner. ^{1}H MRI was acquired with subjects in breath-hold position using a whole-body radiofrequency coil and a ^{1}H fast-spoiled gradient-recalled echo (FGRE) sequence with a partial echo (total data acquisition time = 12 seconds; repetition time [TR]/echo time [TE]/flip-angle = 4.3 ms/1.0 ms/30°; field-of-view [FOV] = 40 × 40 cm; matrix = 128 × 80 [zero-padded to 128 × 128]; partial echo percent = 62.5%; bandwidth [BW] = 62.50 kHz; number of excitations [NEX] = 1; number of slices = 14; slice thickness = 15 mm). For all MRI breath-hold maneuvers, oxygen saturation (S_PO_2) was continuously monitored using a digital pulse oximeter.

Hyperpolarized ^{3}He MRI was performed using a single-channel rigid elliptical transmit-receive chest coil (RAPID Biomedical, Rimpar, Wuerzburg, Germany). A polarizer system (HeliSpin; Polarean, Durham, NC) was used to polarize the ^{3}He gas, which achieved polarization levels of approximately 40%. Doses of 5 mL/kg of body weight were diluted with medical-grade N_2 gas (Spectra Gases, Branchburg, NJ) and administered in 1.0 L Tedlar bags (Jensen Inert Products,

Coral Springs, FL). Hyperpolarized ^{3}He ventilation images were acquired with subjects in breath-hold position after inspiration of a 1.0 L ^{3}He/N_2 mixture using an FGRE method with a partial echo (total data acquisition time = 10 seconds; TR/TE/flip-angle = 3.8 ms/1.0 ms/7°; FOV = 40 × 40 cm; matrix = 128 × 80 (zero-padded to 128 × 128); partial echo percent = 62.5%; BW = 62.50 kHz; NEX = 1; number of slices = 14; slice thickness = 15 mm). The flip angle was determined using a constant flip-angle approach where flip angle (α) depends on the number of phase encoding steps (Y-gradient steps). Thus, $\alpha = \tan^{-1}\sqrt{2/N}$, where N was the number of Y-gradient steps. Therefore, for this pulse sequence, where there are 128 Y-gradient steps, a 7.12° flip angle was used. Hyperpolarized ^{3}He diffusion-weighted images were acquired using an FGRE sequence with centric *k*-space sampling (total data acquisition time = 14 seconds; TR/TE/flip-angle = 6.8 ms/4.5 ms/8°; FOV = 40 × 40 cm; matrix = 128 × 128; BW = 62.50 kHz; NEX = 1; number of slices = 7; slice thickness = 30 mm). Two interleaved images were acquired with and without additional diffusion sensitization (G = 1.94 G/cm; b = 1.6 s/cm^2; rise-and-fall time = 0.5 ms; gradient duration = 0.46 ms; diffusion time = 1.46 ms).

Dynamic-free tidal-breathing ^{1}H MRI was acquired over a period of 125 seconds at a rate of four frames per second using an optimized balanced steady state–free precession sequence and respiratory bellows. We used a fast imaging using steady state pulse sequence [FIESTA; GEHC] with total data acquisition time = 125 seconds; TE/TR/flip-angle = 0.6 ms/1.9 ms/15°; FOV = 40 × 40 cm; matrix = 256 × 256; BW = 250 kHz; NEX = 1; number of phases = 500; slice thickness = 15 mm), and a 32-channel torso coil (GEHC). A single coronal slice was obtained with slice thickness = 15 mm. The number of phases refers to the number of images acquired from one specific location over time. In other words, we acquired multiple frames of one single coronal slice over a certain time span. The slice was prescribed on an axial localizer and was positioned slightly posterior to the cardiac silhouette in an effort to eliminate artifacts due to cardiac motion but allow visualization of the aorta.

CT was acquired using a 64-slice LightSpeed VCT scanner (GEHC) at FRC + 1.0 L of N_2 gas using a spiral acquisition (detector configuration = 64 × 0.625 mm; peak x-ray tube voltage = 120 kVp; effective x-ray tube current = 100 mA; x-ray tube rotation time = 500 ms; pitch = 1.0). Image reconstruction was performed using a standard convolution kernel of 1.25 mm.

Image Analysis

Segmentation of ^{3}He MRI and FDMRI ventilation was performed using custom software generated using MATLAB R2013a (Mathworks, Natrick, MA), as previously described (26). ^{3}He MRI apparent diffusion coefficient (ADC) maps were generated as previously described (36). The relative area of the CT density histogram with attenuation values <−950 HU (RA_{950}) was determined using MATLAB R2013a (Mathworks). Pulmonary Workstation 2.0 (VIDA Diagnostics Inc., Coralville, IA) was used to quantify WA% and LA.

Image analysis of dynamic free-breathing ^{1}H MRI was performed using MATLAB R2013a (Mathworks). Nonrigid registration was used to coregister the temporal series of tidal-breathing ^{1}H MRI slices using a modality independent neighborhood descriptor deformable registration method (37). A specific reference image was used so that the corresponding lung volume was consistent with ^{3}He MRI volumes. Pulmonary voxel intensities from the registered free-breathing ^{1}H MRI were aligned along a time axis, and discrete Fourier transforms were performed on the signal intensity oscillation pattern. The frequency of the first ventilation harmonic (corresponding to the respiratory rate) was determined for every voxel, the magnitude of which was used to generate a ventilation map.

The Dice similarity coefficient (DSC) (38) was used to quantify the regional overlap for ^{3}He MRI and FDMRI ventilation, as well as the spatial relationship of CT RA_{950} density maps with FDMRI ventilation defect volume.

TABLE 1. Subject Demographic and Pulmonary Function Measurements

Mean (±SD)	All (*n* = 26)	Bronchiectasis (*n* = 14)	COPD (*n* = 12)	Significant Difference (*P* Value)
Age, years	69 (10)	70 (11)	67 (9)	.5
Male, *n*	11	4	7	—
BMI, (kg·m^{-2})	25 (4)	23 (4)	27 (4)	.02
Pack years	31 (40)	4 (10)	63 (39)	<.001
FEV_1, $\%_{pred}$	64 (22)	68 (22)	60 (23)	.4
FVC, $\%_{pred}$	82 (22)	73 (20)	91 (22)	.04
FEV_1/FVC, %	60 (16)	70 (12)	50 (14)	.001
TLC, $\%_{pred}$	107 (18)	98 (14)	117 (16)	.003
RV/TLC, %	51 (10)	54 (11)	49 (9)	.3
R_{aw}, $\%_{pred}$	138 (41)	135 (48)	141 (33)	.7
DL_{CO}, $\%_{pred}$	57 (19)	60 (18)	53 (21)	.3

BMI, body mass index; COPD, chronic obstructive pulmonary disease; DL_{CO}, diffusing capacity of lung for carbon monoxide; FEV_1, forced expiratory volume in 1 second; FVC, forced vital capacity; $\%_{pred}$, percent of predicted value; R_{aw}, airways resistance; RV, residual volume; SD, standard deviation; TLC, total lung capacity.

Significant difference between subgroups ($P < .05$) determined by the analysis of variance.

Statistics

Independent *t* tests, tests for normality (determined with a Shapiro–Wilk test), and analysis of variance with post hoc analysis using the Holm–Bonferroni correction were performed using SPSS Statistics, V22.0 (SPSS Inc., Chicago, IL). Pearson correlation coefficients (r) were used to determine the correlation between measurements using SPSS Statistics, V22.0 (SPSS Inc.). Measurement agreement was

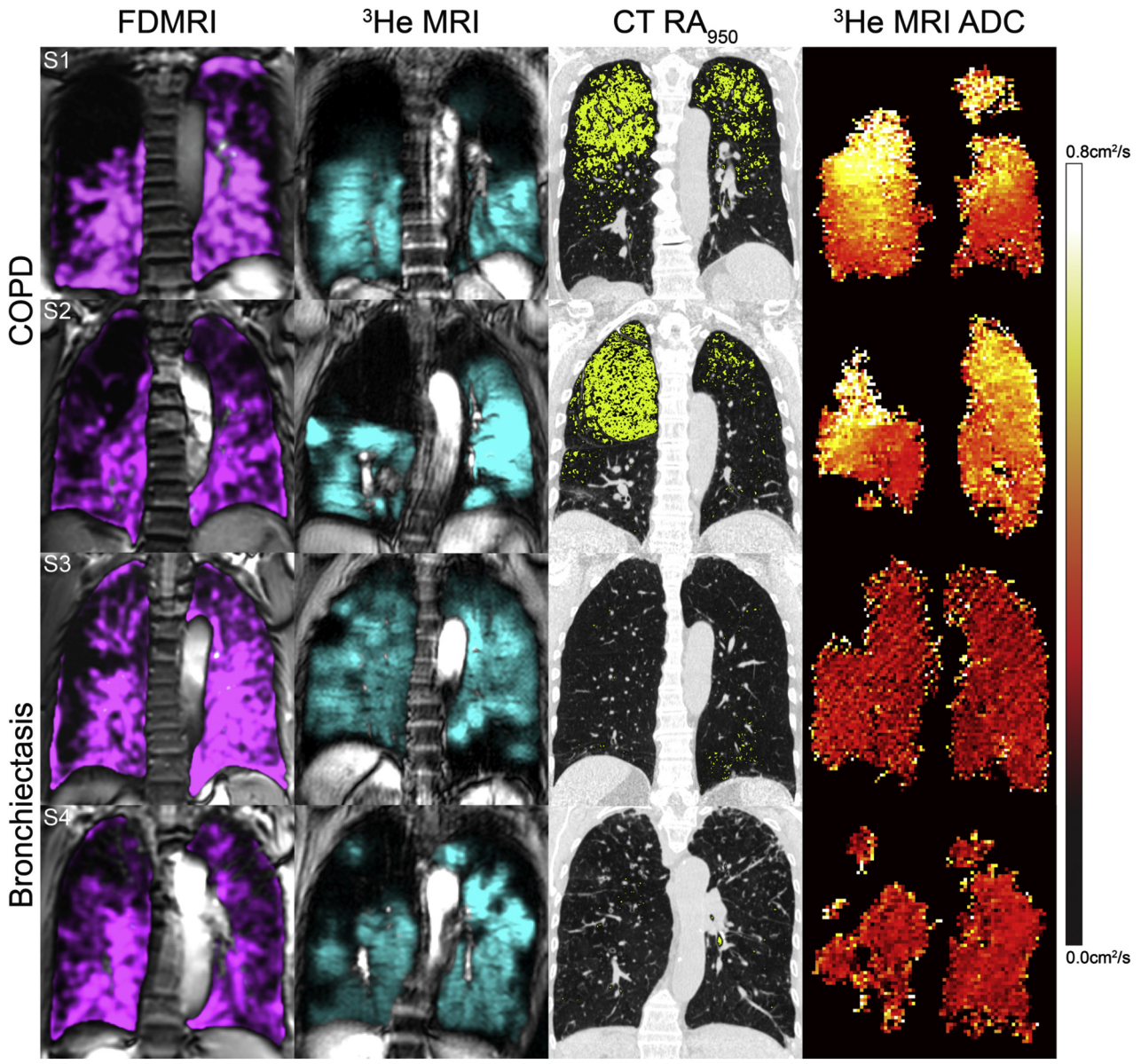

Figure 1. Ventilation and computed tomography (CT) imaging for representative COPD and bronchiectasis subjects. Free-breathing ^{1}H magnetic resonance imaging (FDMRI) in *magenta* coregistered with ^{1}H MRI. ^{3}He MRI static ventilation in *aqua* coregistered with ^{1}H MRI. CT density masks where *yellow* = attenuation < −950 Hounsfield units (RA_{950}) and ^{3}He MRI apparent diffusion coefficient maps, both reflective of emphysema for subjects with chronic obstructive pulmonary disease (S1 and S2) and bronchiectasis (S3 and S4). ADC, apparent diffusion coefficient; COPD, chronic obstructive pulmonary disease; CT, computed tomography; FDMRI, free-breathing ^{1}H magnetic resonance imaging; MRI, magnetic resonance imaging; RA_{950}, relative area of the lung with attenuation values <−950 HU.

evaluated using the Bland–Altman method using GraphPad Prism v6.0 (GraphPad Software Inc., La Jolla, CA). Correlation coefficients were compared using the Fisher z′ transformation for each r value (21). Results were considered significant when the probability of two-tailed type I error was <5% ($P < .05$).

RESULTS

Table 1 shows the demographic and pulmonary function test measurements for all subjects (69 ± 10 years), as well as the 12 subjects with COPD (67 ± 9 years) and 14 with bronchiectasis (70 ± 11 years). For subjects with COPD, three were GOLD grade I, four were GOLD grade II, and five were GOLD grades III/IV. CT evidence of emphysema only was reported in seven subjects with COPD, and there was CT evidence of both emphysema and bronchiectasis in five subjects with COPD.

Figure 1 shows coronal FDMRI and ^{3}He MRI ventilation registered to the ^{1}H MRI of the thorax, as well as RA_{950} and ^{3}He ADC maps for two subjects representative of COPD and two subjects representative of bronchiectasis. As shown in

TABLE 2. Imaging Measurements

Mean (±SD)	All (n = 26)	Bronchiectasis (n = 14)	COPD (n = 12)	Significant Difference (P Value)
FDMRI Ventilation, %	94 (4)	95 (3)	93 (6)	.3
^{3}He MRI Ventilation, %	79 (12)	82 (9)	76 (14)	.2
FDMRI VDP, %	6 (4)	5 (3)	7 (6)	.3
^{3}He MRI VDP, %	21 (12)	18 (9)	24 (14)	.2
^{3}He MRI ADC, cm^2/s	0.35 (0.13)	0.27 (0.05)	0.43 (0.12)	<.001
CT RA_{950}, %	5 (7)	2 (3)	9 (8)	.005
CT WA, %	57 (2)	58 (2)	56 (2)	.009
CT LA, mm^2	46 (14)	40 (10)	53 (15)	.01

ADC, apparent diffusion coefficient; COPD, chronic obstructive pulmonary disease; CT, computed tomography; FDMRI, free-breathing ^{1}H magnetic resonance imaging; LA, lumen area; MRI, magnetic resonance imaging; RA_{950}, relative area of the lung with attenuation values <−950 HU; SD, standard deviation; VDP, ventilation defect percent; WA, wall area.

Significant difference between groups (P < .05) determined by the analysis of variance.

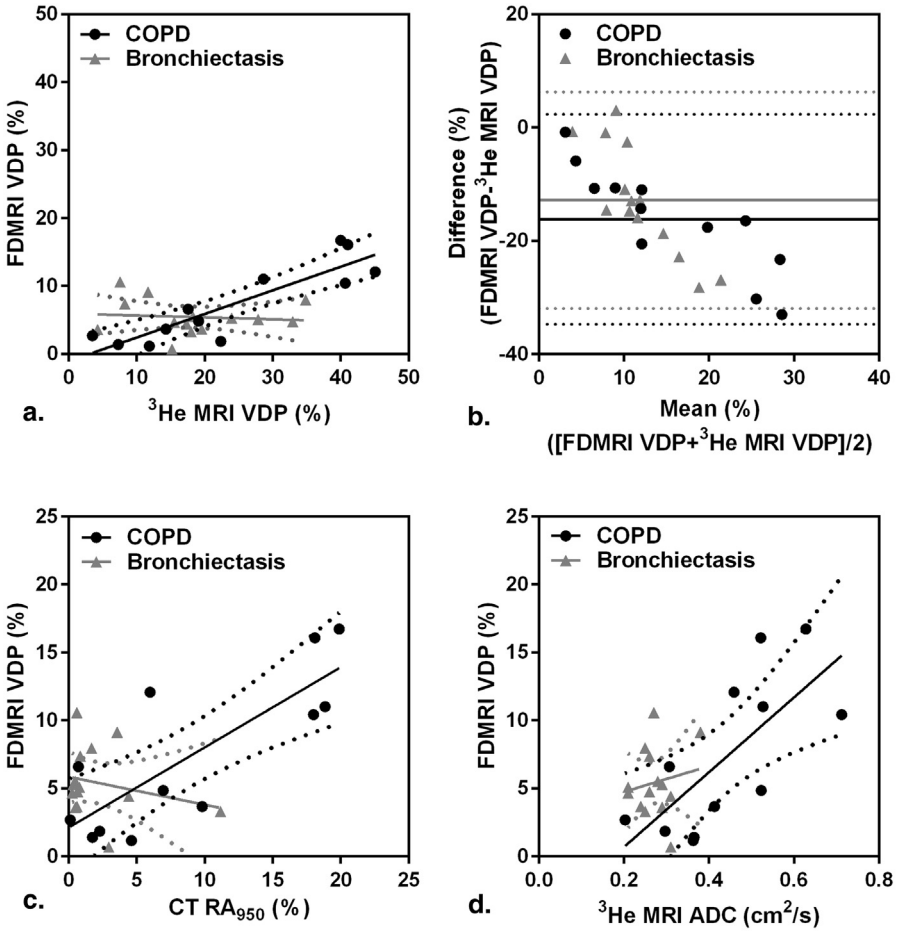

Figure 2. Correlations for free-breathing ^{1}H magnetic resonance imaging (FDMRI) with ^{3}He MRI and computed tomography (CT) relative area of the lung with attenuation values <−950 HU (RA_{950}). **(a)** FDMRI ventilation defect percent (VDP) linear regression with ^{3}He MRI VDP (chronic obstructive pulmonary disease [COPD], r = 0.88; r^2 = 0.78; P = .0001; y = 0.35x − 1.07 and bronchiectasis, r = −0.1; r^2 = 0.009; P > .05; y = −0.03x + 5.92), **(b)** Bland–Altman analysis of agreement for FDMRI and ^{3}He MRI VDP (COPD, bias = −16 ± 9%; lower limit = −35%; upper limit = 2% and bronchiectasis, bias = −13 ± 10%; lower limit = −32%; upper limit = 6%), **(c)** FDMRI VDP linear regression with CT RA_{950} (COPD, r = .80; r^2 = .64; P = .002; y = 0.59x + 2.10 and bronchiectasis, r = −0.23; r^2 = 0.05; P > .05; y = −.21x + 5.85), **(d)** FDMRI VDP linear regression with ^{3}He MRI apparent diffusion coefficient (COPD, r = 0.71; r^2 = 0.51; P = .01; y = 28x + 5 and bronchiectasis, r = .16; r^2 = .03; P > .05; y = 9.4x + 2.9). *Dotted lines* = 95% confidence intervals. ADC, apparent diffusion coefficient; COPD, chronic obstructive pulmonary disease; CT, computed tomography; FDMRI, free-breathing ^{1}H magnetic resonance imaging; MRI, magnetic resonance imaging; RA_{950}, relative area of the lung with attenuation values <−950 HU; VDP, ventilation defect percent.

Figure 1, for all four subjects, there were qualitatively similar ventilation patterns derived from FDMRI and ^{3}He MRI. In subjects with COPD, regional ventilation defects were also qualitatively similar to regional emphysema apparent in the RA_{950} density maps and the brighter regions of ^{3}He MRI ADC maps.

Table 2 provides imaging measurements for subjects with COPD and bronchiectasis. FDMRI (94 ± 4%) and ^{3}He MRI (79 ± 12%) ventilation measurements were significantly different (P < .001). FDMRI VDP (6 ± 4%) was also significantly different than ^{3}He MRI VDP (21 ± 12%; P < .001). As expected, ^{3}He MRI ADC was significantly greater in subjects with COPD as compared to those with bronchiectasis (P < .001), and all CT measurements (RA_{950}, WA%, and LA) were significantly greater in subjects with COPD as compared to those with bronchiectasis.

Figure 2 shows the linear correlation of FDMRI with ^{3}He MRI VDP and the agreement between measurements for subjects with COPD and bronchiectasis. Although FDMRI and ^{3}He MRI VDP were significantly different, as shown in Table 2, these measurements were strongly correlated in subjects with COPD (r = .88; P = .0001), but not in those with bronchiectasis (r = .1; P > .05). Bland–Altman analysis showed a bias of −16 ± 9% (95% confidence interval, −35% to 5%) for FDMRI (Fig 2b), and this bias increased with increasing VDP for subjects with COPD. FDMRI VDP was also strongly correlated with RA_{950} (r = .80; P = .002) and ^{3}He MRI ADC (r = .71; P = .01) for subjects with COPD, both of which are well-established measurements of emphysema (8,16).

Given the strong correlation between FDMRI and ^{3}He MRI VDP for subjects with COPD, we evaluated the spatial relationships for ventilation and ventilation defects derived from using both these methods. These data are shown in Table 3 and for the subjects representative of COPD (S1 and S2) and bronchiectasis (S3 and S4) in Figure 3. Table 3 provides mean DSC for FDMRI and ^{3}He MRI ventilation and ventilation defects. The DSC for FDMRI and ^{3}He MRI ventilation was 86% for both subject groups. In a similar fashion, the spatial overlap of FDMRI ventilation with lung regions >−950 HU was 92% and 93% for subjects with COPD and bronchiectasis, respectively. For ventilation defects, the spatial relationship of FDMRI and ^{3}He MRI ventilation defects was 20 ± 17% and 14 ± 9% for subjects with COPD and bronchiectasis, respectively. In subjects with COPD, the DSC for FDMRI ventilation defects with lung regions <−950 HU, reflective of emphysema was 19 ± 20%. For subjects with bronchiectasis, the spatial overlap of FDMRI and lung regions <−950 HU (2 ± 3%) was significantly lower than the spatial overlap of FDMRI and ^{3}He MRI ventilation defects (14 +/− 9% P < .001).

Some of these spatial relationships are also shown in Figure 3, where the regional similarities of FDMRI with ^{3}He static ventilation images are visually apparent for subjects with COPD (S1 and S2) and less obvious for those with bronchiectasis (S3 and S4). In particular for the subjects with bronchiectasis, there is little evidence of emphysema, and therefore, there is negligible overlap between RA_{950} and ventilation defects.

Table 4 summarizes the significant correlations for FDMRI VDP with ^{3}He MRI, CT, and pulmonary function measurements for the COPD and bronchiectasis subgroups. There were significant correlations for FDMRI VDP with ^{3}He MRI VDP and ADC, R_{aw}, and RA_{950} (P < .05) for subjects with COPD. For subjects with bronchiectasis, there was a significant correlation between FDMRI VDP and LA (P < .05). For those with COPD, the FDMRI and ^{3}He MRI VDP correlations were not significantly different; however, for subjects with bronchiectasis, there were significant differences.

TABLE 3. Quantitative Spatial Relationships for FDMRI Ventilation and Ventilation Defects

Mean DSC (±SD)	All (n = 26)	Bronchiectasis (n = 14)	COPD (n = 12)	Significant Difference (P Value)
Ventilation				
FDMRI–^{3}He MRI, %	86 (5)	86 (4)	86 (7)	.8
FDMRI–$RA_{>950}$, %	92 (3)	93 (2)	92 (3)	.5
Ventilation defects				
FDMRI–^{3}He MRI, %	16 (13)	14 (9)	20 (17)	.2
FDMRI–RA_{950}, %	10 (16)	2 (3)	19 (20)	.005

ADC, apparent diffusion coefficient; DSC, Dice similarity coefficient; FDMRI, free-breathing ^{1}H magnetic resonance imaging; MRI, magnetic resonance imaging; RA_{950}, relative area <−950 HU; $RA_{>950}$, relative area >−950 HU; VDP, ventilation defect percent.

Significant difference between groups (P < .05) determined by the analysis of variance.

DISCUSSION

In this proof-of-concept study, we evaluated 26 patients including 12 subjects with COPD and another 14 with bronchiectasis and observed the following: 1) in all subjects, FDMRI VDP was significantly less than ^{3}He MRI VDP, 2) in subjects with COPD but not in those with bronchiectasis, FDMRI and ^{3}He MRI ventilation and VDP were quantitatively correlated, and these values showed strong spatial relationships with one another and with RA_{950} maps, and 3) in subjects with COPD only, there were significant and similar correlations for FDMRI and ^{3}He MRI VDP with pulmonary function test and CT measurements.

In all subjects, FDMRI VDP was significantly less than ^{3}He MRI VDP. It is difficult to completely understand why FDMRI VDP was significantly less and FDMRI ventilation was significantly greater than ^{3}He MRI measurements in all subjects. However, one explanation may be derived from the underlying principles of the two methods and how they generate or capture ventilation information. Inhaled contrast gas methods provide static breath-hold snapshots of where the high-contrast inhaled gas travels to and resides during the scanning period of 8–15 seconds. In this manner, very high-contrast and signal-to-noise ventilation images can be easily generated and processed. In contrast, but similar to four-dimensional CT (4DCT) that produces three-dimensional image data sets through time (39,40), FDMRI generates ventilation contrast based on image signal differences during the breathing cycle as air enters and leaves the pulmonary system and tissue contracts and expands. This is a more indirect approach that relies on robust and accurate image processing methods to coregister the dynamic free tidal-breathing ^{1}H MRI. This method also relies on the inherent image signal intensity and signal-to-noise ratios of pulmonary images from a system that is

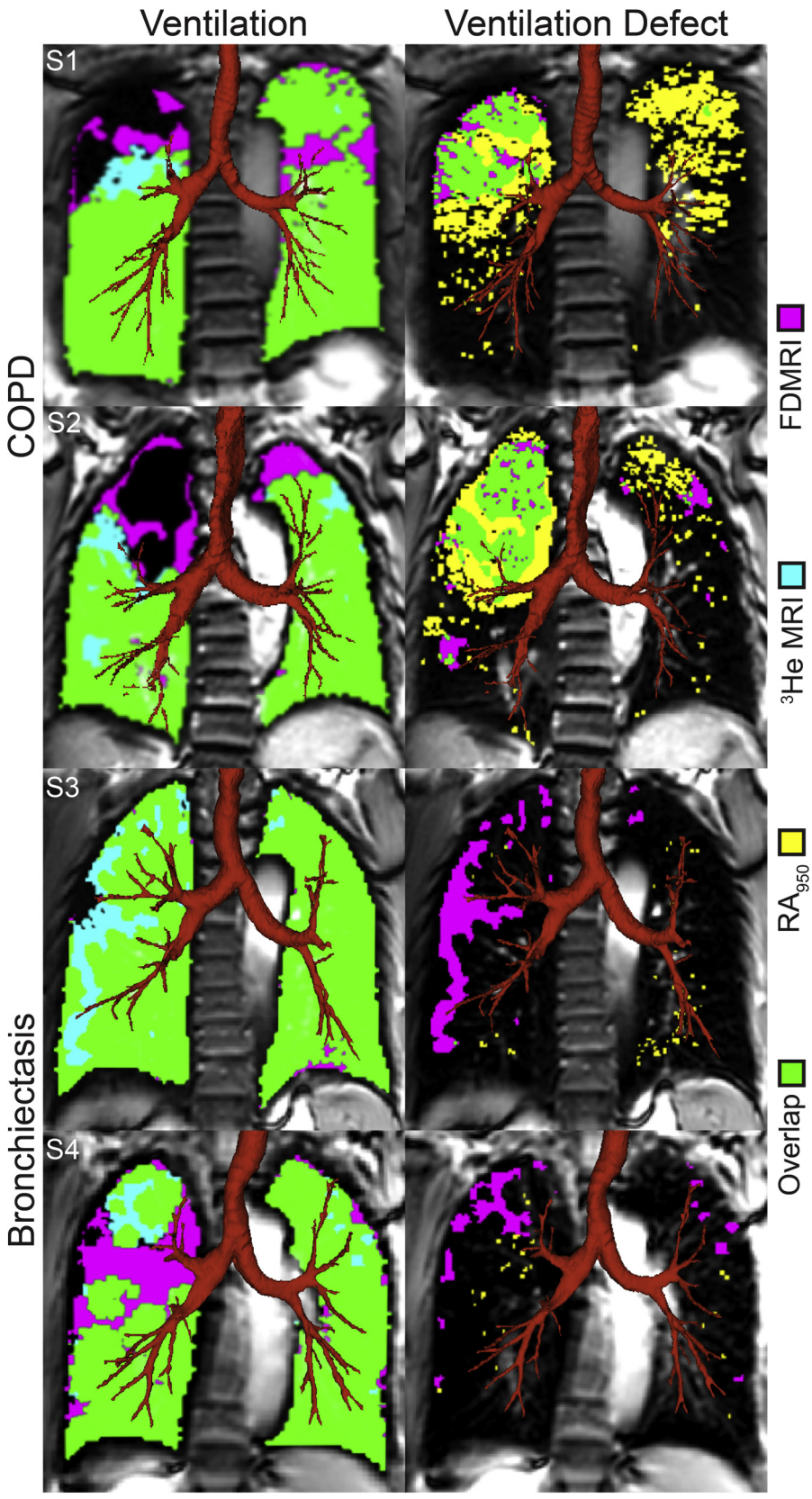

Figure 3. Spatial relationships of free-breathing ^{1}H magnetic resonance imaging (FDMRI) with ^{3}He MRI ventilation and emphysema for representative subjects with chronic obstructive pulmonary disease (COPD) and bronchiectasis. Left panel: spatial overlap (*green*) of FDMRI (*magenta*) and ^{3}He MRI (*aqua*) ventilation coregistered with ^{1}H MRI and airway tree in *brown*. Right panel: spatial overlap (*green*) of FDMRI (*magenta*) ventilation defects and relative area of the lung with attenuation values <−950 HU (RA$_{950}$) mask (*yellow*) coregistered with CT for subjects with COPD (S1 and S2) and bronchiectasis (S3 and S4). Dice coefficients for FDMRI–^{3}He MRI ventilation, S1 = 88%; S2 = 86%; S3 = 91%; S4 = 84% and FDMRI defects: RA$_{950}$, S1 = 41%; S2 = 56%; S3 = 1%; S4 = 0%. COPD, chronic obstructive pulmonary disease; FDMRI, free-breathing ^{1}H magnetic resonance imaging; RA$_{950}$, relative area of the lung with attenuation values <−950 HU.

inherently air filled. In CT, the attenuation values for air as compared to tissue provide significant contrast. However, the contrast derived from the ^{1}H signal changes are inherently weak, and this certainly necessitates that the image processing methods used be more complex and robust. Previous work (41) explored the spatial and quantitative relationship of ^{3}He

TABLE 4. Pearson Correlations for FDMRI and ^{3}He MRI

	FDMRI VDP %		^{3}He MRI VDP %		Fisher z′	
	Bronchiectasis (n = 14)	COPD (n = 12)	Bronchiectasis (n = 14)	COPD (n = 12)	B	C
	r/*P* Value	r/*P* Value	r/*P* Value	r/*P* Value	*P* Value	*P* Value
FEV_1, $\%_{pred}$	0.41/.1	−0.22/.5	−0.73/.003	−0.42/.2	.001	.6
FVC, $\%_{pred}$	0.31/.3	0.20/.5	−0.60/.02	−0.04/.9	.02	.7
RV/TLC, %	−0.31/.3	−0.19/.6	0.65/.02	−0.07/.8	.01	.8
R_{aw}, $\%_{pred}$	−0.23/.4	0.60/.04	0.47/.09	0.56/.06	.08	.9
DL_{CO}, $\%_{pred}$	0.08/.8	−0.57/.05	−0.36/.2	−0.61/.04	.3	.9
FDMRI ventilation, %	∼−1/<.001	∼−1/<.001	0.1/.7	−0.88/<.001	<.001	<.001
FDMRI VDP, %	—/—	—/—	−0.1/.7	0.88/<.001	—	—
^{3}He MRI ventilation, %	0.1/.7	−0.88/<.001	∼−1/<.001	∼−1/<.001	<.001	<.001
^{3}He MRI VDP, %	−0.10/.7	0.88/<.001	—/—	—/—	—	—
^{3}He MRI ADC, cm^2/s	0.16/.6	0.71/.01	0.35/.2	0.76/.004	.6	.8
CT RA_{950}, %	−0.23/.4	0.80/.002	−0.04/.9	0.72/.008	.6	.7
CT WA, %	−0.35/.2	−0.07/.8	0.29/.3	−0.18/.6	.1	.8
CT LA, mm^2	0.58/.03	0.43/.2	−0.09/.7	0.59/.04	.08	.6

ADC, apparent diffusion coefficient; DL_{CO}, diffusing capacity for carbon monoxide; FEV_1, forced expiratory volume in 1 second; FDMRI, free-breathing ^{1}H magnetic resonance imaging; FVC, forced vital capacity; LA, lumen area; $\%_{pred}$, percent of predicted value; MRI, magnetic resonance imaging; r, Pearson correlation coefficients; R_{aw}, airways resistance; RA_{950}, relative area of the lung with attenuation < −950 HU; RV/TLC, residual volume/total lung capacity; VDP, ventilation defect percent; WA, wall area.

MRI and 4DCT ventilation measurements in a proof-of-concept demonstration in a small number of non–small cell lung cancer patients. There was excellent spatial correspondence for the ventilation maps derived using static MRI and free-breathing CT imaging approaches with no significant differences in ventilation. These results provided good evidence that ventilation maps and measurements generated using vastly different image acquisition and analysis methods, as well as breathing maneuvers, provided similar regional and quantitative ventilation information.

It is important to note that ^{3}He MRI ventilation percent and VDP are not independent measurements because these simply sum to 100%. However, because here we are directly comparing VDP, which is a relatively small volume and ventilation which is a large volume for both Fourier decomposition (FD) and ^{3}He MRI, we think it is important to use and compare both values. This is especially important to show spatial relationships such as the Dice similarity coefficient that is highly dependent on the relative size of the comparators. We think this is also important because the ^{3}He ventilation MRI depicts gas distribution, whereas the FDMRI ventilation reflects the ventilation fundamental frequency and signal intensity changes related to this value. Because of this, spatial overlap analyses were conducted for both ventilation maps and ventilation defect maps obtained using both ^{3}He and FDMRI.

In subjects with COPD but not in those with bronchiectasis, FDMRI and ^{3}He MRI ventilation were quantitatively and spatially related. In addition, FDMRI and ^{3}He MRI VDP were quantitatively correlated and showed strong spatial relationships with RA_{950} maps—those regions that reflected emphysematous destruction or air in CT images. We were surprised to observe such differences in the spatial and quantitative correlations for FDMRI and ^{3}He MRI in subjects with COPD as compared to those with bronchiectasis. One explanation can be derived from the presence of thick mucus (which appears as greater ^{1}H signal intensity relative to that of lung parenchyma) in the airways and parenchyma in bronchiectasis that may lead to registration error. To generate FDMRI ventilation images, registration algorithms must account for the movement of the diaphragm, and any registration error will result in regions of high signal intensity (eg, mucus pooling in subjects with bronchiectasis) oscillating at the same frequency as respiration. This registration error can result in apparently increased ventilation, which may or may not accurately reflect truly ventilated regions. Thus, in subjects with bronchiectasis, there may be regions that appear as ventilation in FDMRI that are in fact not ventilated because of misalignment of the mucus' boundaries via the deformable registration process. We must acknowledge that all three imaging methods measure very different physical parameters. For example, although CT provides a measurement of regional lung tissue density, ^{3}He MRI provides a functional estimate of pulmonary ventilation and alveolar dimensions using diffusion-weighted imaging. FDMRI on the other hand, provides an estimate of ventilation by quantifying the signal intensity contributions throughout the compression and expansion of the lung parenchyma via the cardiac and the respiratory cycles. However, we recently showed that in subjects with COPD, ^{3}He MRI ventilation defects often colocalize with large emphysematous bullae (42). In fact, we previously observed this in patients with advanced emphysema and because of this work hypothesized that this spatial colocalization was related to the long time constants for filling of emphysematous bullae and not airways disease. Here, and in light of these previous findings, we directly evaluated the

spatial colocalization of emphysematous regions with FDMRI and ^{3}He MRI ventilation defects. The spatial relationships observed for FDMRI and ^{3}He MRI ventilation defects with RA_{950} in the present study suggest that in patients with emphysema, ventilation defects generated using FDMRI may also be derived to the long time constants for lung filling. Our findings further support the notion that these methods (ie, FDMRI, ^{3}He MRI, and CT), although very different, are probing and interrogating similar functional, but likely not structural information, in subjects with COPD. It appears that a free-breathing method like FDMRI, shows some dependence on the very long time constants for filling emphysematous bullae, and this finding should be considered when using FDMRI for COPD imaging.

Finally, only in subjects with COPD, there were significant and similar correlations for FDMRI and ^{3}He MRI VDP with pulmonary function test and CT measurements. These are important findings that further support and suggest that both methods provide similar functional information in subjects with COPD even though they are very unique methods. In contrast, for those with bronchiectasis, there was a significant correlation between FDMRI VDP and airway LA. This suggests that elevated LA (corresponding to dilated airways) may be related to low proton density.

We recognize and acknowledge that this work was limited by the relatively small sample size. In addition, we studied mainly subjects with moderate COPD (8 of 12 subjects with GOLD grade II or III), and given our understanding of the heterogeneity of patients with COPD, caution should be used when extrapolating our results to a broader COPD group. Fourier decomposition has recently emerged as a pulmonary functional MRI method, with the promise of serial lung function measurements without a dependence on polarized or other inhaled gases or multinuclear capabilities. This opens up the opportunity for functional lung imaging on conventional MRI scanners—available more universally, albeit the final measurements are dependent on more sophisticated image processing methods. It should be noted that one of the challenges associated with pulmonary proton MRI methods is the weak pulmonary proton signal intensity that is further diminished at higher field strengths because of the relationship between field strength and $T2^\star$ effects. Previous pilot and development studies at 1.5 T have shown qualitative agreement for regional ventilation and perfusion measurements with the clinical reference standard SPECT/CT (28). Moreover, recent studies have also demonstrated the reproducibility of FDMRI ventilation-weighted and perfusion-weighted images in healthy volunteers (32). Finally FDMRI-to-^{3}He MRI comparisons in animals showed similar regional abnormalities including pulmonary embolism, atelectasis, and air trapping (30).

To our knowledge, there has been no prospective comparison of FDMRI to ^{3}He MRI at 3 T in subjects with COPD and bronchiectasis. Consistent with previous studies, we showed similar regional ventilation abnormalities using FDMRI and ^{3}He MRI in subjects with COPD, and these appear to be dominated by the presence of regional emphysematous bullae. In summary, FDMRI and ^{3}He MRI ventilation and VDP were strongly correlated in subjects with COPD but not in those with bronchiectasis. Only in subjects with COPD, FDMRI ventilation defects were also spatially related with ^{3}He MRI ventilation defects and CT measurements of emphysema.

ACKNOWLEDGMENTS

The authors thank Sandra Blamires, CCRC, for clinical coordination; Andrew Wheatley, BSc, for production and dispensing of ^{3}He gas; and Trevor Szekeres, RTMR, for magnetic resonance imaging of research volunteers.

REFERENCES

1. Vestbo J, Hurd SS, Agusti AG, et al. Global strategy for the diagnosis, management, and prevention of chronic obstructive pulmonary disease: GOLD executive summary. Am J Respir Crit Care Med 2013; 187(4): 347–365.
2. Pauwels RA, Buist AS, Calverley PM, et al. Global strategy for the diagnosis, management, and prevention of chronic obstructive pulmonary disease. NHLBI/WHO Global Initiative for Chronic Obstructive Lung Disease (GOLD) Workshop summary. Am J Respir Crit Care Med 2001; 163(5): 1256–1276.
3. Vestbo J, Anderson W, Coxson HO, et al. Evaluation of COPD longitudinally to identify predictive surrogate end-points (ECLIPSE). Eur Respir J 2008; 31(4):869–873.
4. Cerveri I, Corsico AG, Accordini S, et al. Underestimation of airflow obstruction among young adults using FEV1/FVC <70% as a fixed cut-off: a longitudinal evaluation of clinical and functional outcomes. Thorax 2008; 63(12):1040–1045.
5. Enright PL, Kaminsky DA. Strategies for screening for chronic obstructive pulmonary disease. Respir Care 2003; 48(12):1194–1201. discussion 201–3.
6. Hackx M, Bankier AA, Gevenois PA. Chronic obstructive pulmonary disease: CT quantification of airways disease. Radiology 2012; 265(1): 34–48.
7. Nakano Y, Muller NL, King GG, et al. Quantitative assessment of airway remodeling using high-resolution CT. Chest 2002; 122(6):271s–275s.
8. Hayhurst MD, MacNee W, Flenley DC, et al. Diagnosis of pulmonary emphysema by computerised tomography. Lancet 1984; 2(8398): 320–322.
9. Klein JS, Gamsu G, Webb WR, et al. High-resolution CT diagnosis of emphysema in symptomatic patients with normal chest radiographs and isolated low diffusing capacity. Radiology 1992; 182(3):817–821.
10. Müller N, Staples C, Miller R, et al. "Density mask". An objective method to quantitate emphysema using computed tomography. Chest 1988; 94(4): 782.
11. Uppaluri R, Mitsa T, Sonka M, et al. Quantification of pulmonary emphysema from lung computed tomography images. Am J Respir Crit Care Med 1997; 156(1):248–254.
12. Zach JA, Newell JD, Jr, Schroeder J, et al. Quantitative computed tomography of the lungs and airways in healthy nonsmoking adults. Invest Radiol 2012; 47(10):596–602.
13. Galban CJ, Han MK, Boes JL, et al. Computed tomography-based biomarker provides unique signature for diagnosis of COPD phenotypes and disease progression. Nat Med 2012; 18(11):1711–1715.
14. O'Brien C, Guest PJ, Hill SL, et al. Physiological and radiological characterisation of patients diagnosed with chronic obstructive pulmonary disease in primary care. Thorax 2000; 55(8):635–642.
15. Patel IS, Vlahos I, Wilkinson TM, et al. Bronchiectasis, exacerbation indices, and inflammation in chronic obstructive pulmonary disease. Am J Respir Crit Care Med 2004; 170(4):400–407.
16. de Lange EE, Mugler JP, 3rd, Brookeman JR, et al. Lung air spaces: MR imaging evaluation with hyperpolarized 3He gas. Radiology 1999; 210(3): 851–857.

17. Kauczor HU, Hofmann D, Kreitner KF, et al. Normal and abnormal pulmonary ventilation: visualization at hyperpolarized He-3 MR imaging. Radiology 1996; 201(2):564–568.
18. Albert MS, Cates GD, Driehuys B, et al. Biological magnetic resonance imaging using laser polarized 129Xe. Nature 1994; 370(6486):199–201.
19. Mathew L, Kirby M, Etemad-Rezai R, et al. Hyperpolarized ^{3}He magnetic resonance imaging: preliminary evaluation of phenotyping potential in chronic obstructive pulmonary disease. Eur J Radiol 2011; 79(1):140–146.
20. Kirby M, Svenningsen S, Kanhere N, et al. Pulmonary ventilation visualized using hyperpolarized helium-3 and xenon-129 magnetic resonance imaging: differences in COPD and relationship to emphysema. J Appl Physiol 2013; 114(6):707–715.
21. Kirby M, Svenningsen S, Owrangi A, et al. Hyperpolarized 3He and 129Xe MR imaging in healthy volunteers and patients with chronic obstructive pulmonary disease. Radiology 2012; 265(2):600–610.
22. Driehuys B, Martinez-Jimenez S, Cleveland ZI, et al. Chronic obstructive pulmonary disease: safety and tolerability of hyperpolarized 129Xe MR imaging in healthy volunteers and patients. Radiology 2012; 262(1):279–289.
23. Kaushik SS, Cleveland ZI, Cofer GP, et al. Diffusion-weighted hyperpolarized 129Xe MRI in healthy volunteers and subjects with chronic obstructive pulmonary disease. Mag Reson Med 2011; 65(4):1154–1165.
24. Parraga G, Ouriadov A, Evans A, et al. Hyperpolarized 3He ventilation defects and apparent diffusion coefficients in chronic obstructive pulmonary disease: preliminary results at 3.0 Tesla. Invest Radiol 2007; 42(6):384–391.
25. Kirby M, Mathew L, Wheatley A, et al. Chronic obstructive pulmonary disease: longitudinal hyperpolarized (3)He MR imaging. Radiology 2010; 256(1):280–289.
26. Kirby M, Heydarian M, Svenningsen S, et al. Hyperpolarized 3He magnetic resonance functional imaging semiautomated segmentation. Acad Radiol 2012; 19(2):141–152.
27. Bauman G, Puderbach M, Deimling M, et al. Non-contrast-enhanced perfusion and ventilation assessment of the human lung by means of Fourier decomposition in proton MRI. Mag Reson Med 2009; 62(3): 656–664.
28. Bauman G, Lützen U, Ullrich M, et al. Pulmonary functional imaging: qualitative comparison of Fourier decomposition MR imaging with SPECT/CT in porcine lung. Radiology 2011; 260(2):551–559.
29. Bauman G, Puderbach M, Heimann T, et al. Validation of Fourier decomposition MRI with dynamic contrast-enhanced MRI using visual and automated scoring of pulmonary perfusion in young cystic fibrosis patients. Eur J Radiol 2013; 82(12):2371–2377.
30. Bauman G, Scholz A, Rivoire J, et al. Lung ventilation- and perfusion-weighted Fourier decomposition magnetic resonance imaging: in vivo validation with hyperpolarized 3He and dynamic contrast-enhanced MRI. Mag Reson Med 2013; 69(1):229–237.
31. Kjørstad Å, Corteville DM, Fischer A, et al. Quantitative lung perfusion evaluation using Fourier decomposition perfusion MRI. Mag Reson Med 2013; 72:558–562.
32. Lederlin M, Bauman G, Eichinger M, et al. Functional MRI using Fourier decomposition of lung signal: reproducibility of ventilation- and perfusion-weighted imaging in healthy volunteers. Eur J Radiol 2013; 82: 1015–1022.
33. Sommer G, Bauman G, Koenigkam-Santos M, et al. Non-contrast-enhanced preoperative assessment of lung perfusion in patients with non-small-cell lung cancer using Fourier decomposition magnetic resonance imaging. Eur J Radiol 2013; 82(12):e879–e887.
34. Yu J, Xue Y, Song HK. Comparison of lung T2* during free-breathing at 1.5 T and 3.0 T with ultrashort echo time imaging. Mag Reson Med 2011; 66(1): 248–254.
35. Miller MR, Hankinson J, Brusasco V, et al. Standardisation of spirometry. Eur Respir J 2005; 26(2):319–338.
36. Kirby M, Heydarian M, Wheatley A, et al. Evaluating bronchodilator effects in chronic obstructive pulmonary disease using diffusion-weighted hyperpolarized helium-3 magnetic resonance imaging. J Appl Physiol 2012; 112(4):651–657.
37. Heinrich MP, Jenkinson M, Bhushan M, et al. MIND: modality independent neighbourhood descriptor for multi-modal deformable registration. Med Image Anal 2012; 16(7):1423–1435.
38. Dice LR. Measures of the amount of ecologic association between species. Ecology 1945; 26(3):297–302.
39. Guerrero T, Sanders K, Castillo E, et al. Dynamic ventilation imaging from four-dimensional computed tomography. Phys Med Biol 2006; 51(4): 777–791.
40. Castillo R, Castillo E, Martinez J, et al. Ventilation from four-dimensional computed tomography: density versus Jacobian methods. Phys Med Biol 2010; 55(16):4661–4685.
41. Mathew L, Wheatley A, Castillo R, et al. Hyperpolarized (3)He magnetic resonance imaging: comparison with four-dimensional x-ray computed tomography imaging in lung cancer. Acad Radiol 2012; 19(12):1546–1553.
42. Kirby M, Pike D, Coxson HO, et al. Hyperpolarized ^{3}He ventilation defects used to predict pulmonary exacerbations in mild to moderate chronic obstructive pulmonary disease. Radiology 2014;140161.